THE JOURNAL OF PHYSICAL CHEMISTRY A

Subscriber access provided by Northwestern Univ. Library

A: Kinetics, Dynamics, Photochemistry, and Excited States

In-Situ Detoxification of VX Surrogate Profenofos by Doped Titanium-Dioxide Nanoparticles under Illumination at the UV and Visible Ranges

Avraham Dayan, Rotem Mor Yosef, Judith Rishpon, Eran Tuval, and Gideon Fleminger

J. Phys. Chem. A, **Just Accepted Manuscript** • DOI: 10.1021/acs.jpca.9b07492 • Publication Date (Web): 16 Oct 2019

is published by the American Chemical Society. 1155 Sixteenth Street N.W., Washington, DC 20036

In-Situ Detoxification of VX Surrogate Profenofos by Doped Titanium-Dioxide Nanoparticles under Illumination at the UV and Visible Ranges

Avraham Dayan[1], Rotem Mor Yosef[1], Judith Risphon[1], Eran Tuval[1] and Gideon Fleminger*[1]

[1] The School of Molecular Cell Biology and Biotechnology, George S. Wise Faculty of Life Sciences, Tel Aviv University, Ramat Aviv 69978, Israel.

*To whom all corresponding should be made - gidifl@tauex.tau.ac.il

This research was funded by the Israeli Ministry of Defense (Project 4440492583).

The authors declare no competing financial interest.

Abbreviations

AChE – Acetylcholinesterase

A-NP – Anatase Nano Particle

BCP – 4-Bromo-2-ChloroPhenol

Cyt C – Cytochrome c

DPDS – Dipropyl Disulfide

EDS – Energy Dispersive Spectroscopy

GC – Gas Chromatography

HPLC – High Performance Liquid Chromatography

HR-SEM – High-Resolution Scanning Electron Microscope

MS – Mass Spectrometry

PF – Profenofos

ROS – Reactive Oxygen Species

TEM – Transmission Electron Microscopy

TiO_2 – Titanium Dioxide

UV – Ultra-Violet

VIS – Visible

XRD – X-Ray Diffraction

XRF – X-Ray Fluorescence

Abstract

The photocatalytic activity of titanium dioxide (TiO_2) due to the generation of reactive oxygen species (ROS) under UV-excitation is often used for the decontamination of toxic hazardous materials and self-cleaning processes. However, the large band-gap of TiO_2 limits the activity to the UV region. This limitation can be overcome by metal doping, which results in extending TiO_2 activity into the visible range (VIS). This paper describes the preparation and characterization of several TiO_2 forms and their modifications for enhanced photocatalytic activity at the UV-VIS range. In order to advance this concept for environmental decontamination, the degradation of the phosphorous-organic pesticide and chemical warfare agent, profenofos (PF), was tested. Fast and full degradation of PF was achieved using either TiO_2 at the near UV (365 nm) or Ag-doped TiO_2 (TiO_2-Ag) at the UV and VIS ranges (400-550nm). The degradation products were identified chromatographically using GC/MS and HPLC, while the detoxification effect was determined electrochemically using an acetylcholinesterase biosensor. In view of our results we suggest that TiO_2-Ag may be implemented as an additive in surface coatings to allow *in situ* green self-cleaning.

1. Introduction

Organophosphates are common acetylcholinesterase (AChE) inhibitors, used as pesticides in the agricultural industry, as well as chemical warfare agents for military applications [1]. In the case of environmental contamination with these materials, urgent remediation is required. The current decontamination methods, such as bleaching powders, decontamination foams and solution, are often insufficient due to the needed storage, transport and material disposable [2]. This limitation can be overcome by metal oxides such as ZiO_2 [3], CaO [4], TiO_2 [5] as *in situ* decontaminating agents.

The photocatalytic activity of TiO_2 has been widely applied in decontamination processes, particularly in self-cleaning, odor removal, degradation of toxic materials and bacteria annihilation [6]. TiO_2 is particularly suitable for this purpose due to its high photoreactivity, high chemical and physical stabilities, low toxicity and commercial availability at relatively low cost compared to other photocatalytic metal-oxides [7]. The large band-gap of TiO_2 requires excitation at the UV region [8]. Upon UV illumination, excited TiO_2 produces Reactive Oxygen Species (ROS) [9] which plays an important role in the photocatalytic reaction mechanism [10]. When TiO_2 absorbs photons with energies higher than its band-gap, electrons are excited from the valence band into the unoccupied conduction band, which leads to the creation of positively charged holes in the valence band [11]. Excited-state electrons and holes react with water and O_2 molecules that are innately present on metal oxides. Depending upon the exact conditions, the holes, OH• radicals, O_2^-, H_2O_2 and O_2 play an important role in the photocatalytic reaction mechanism [10].

One of the goals for improvement of the performance of TiO_2 nanomaterials is to enhance their photoreactivity applicability by shifting their optical reactivity towards the VIS range, due to the fact that only a small fraction (3-5%) of sunlight radiation falls within the UVA range, usually utilized for photodegradation [12]. Commonly used methods are bulk [10] and surface [13] modifications, which involve either introduction of impurities into the crystal lattice or adsorption of metal species to the surface of the catalyst, leading to the decrease in the band-gap of the catalyst, TiO_2 [14]. Surface modification may also facilitate the attachment to the carrier of other photon-capturing molecules, increasing its photoreactivity [13].

This research is focused on the study and characterization of TiO_2 as a photocatalyst for decontamination of toxic hazards, producing nontoxic products that pose no threat to humans or the environment. Profenofos (PF) is an organophosphorus pesticide that acts by inhibition of acetylcholinesterase activity [15] and often serves as a nerve gas model [2, 16]. In this work, a fast degradation of PF was achieved using TiO_2 at the near UV range (365 nm). The same positive results have been obtained after surface modification of TiO_2 by transition metal deposition with silver atoms (TiO_2-Ag) under illumination at the more desirable VIS scale (400-550nm).

2 Experimental sections

2.1 Materials

All chemicals and carriers were of analytical grade and purchased from Sigma-Aldrich (St. Louise, MO), unless otherwise specified.

2.2 Methods

2.2.1 Catalyst preparation

The preparation of Ag doped titania samples (TiO_2-Ag) was according to [17]. Shortly, 0.2g of TiO_2 was dispersed in 100 ml of distilled water and sonicated for 5 min. followed by the addition of 0.0425g $AgNO_3$. The solution was mixed, adjusting the pH to 10 with NH_4OH (30% in water). For wet-impregnation reduction, 9.4mg of sodium borohydride ($NaBH_4$) in 10 ml of distilled water were added and the solution was mixed for 30 min. The precipitate was collected by centrifugation and dried overnight at temperature 50°C in a dry oven.

2.2.2 X-ray diffraction (XRD)

The X-ray diffraction (XRD) data was acquired using a laboratory standard D8 Advanced X-ray Diffractometer in Bragg-Brentano geometry (supplied by Bruker AXS, Germany) equipping a Cu Kα source and LynxEye detector. The following XRD setting parameters were used: range between 10 and 70 with a step size of 0.05, 0.5s per step, sample rotation of 60 rpm.

2.2.3 X-Ray Fluorescence (XRF)

Chemical analysis was done using a Thermo Scientific NITON energy-dispersive X-ray fluorescence (EDXRF) analyzer, model XL3t XRF. The XL3t XRF analyzer, a handheld device, was mounted in the laboratory configuration to quantify the presence of elements in standard analytical range (from sulfur S16 to Uranium U92)

and additional light elements (Magnesium Mg12, Aluminum Al13, Silicon Si14, and Phosphorus P15 via helium purge) in road dust. The detection limits for all analyses were based on a 130-sec total analysis time in a regular Cu\Zn mining mode.

2.2.4 Diffuse reflectance UV/VIS

For the evaluation of photophysical properties, diffuse reflectance UV-VIS spectra were recorded in the diffuse reflectance mode (R) using a Thermo Scientific Evolution 300 spectrometer equipped with a DRA-EV-300 Integrating Sphere with $BaSO_4$ as a standard.

2.2.5 Scanning electron microscopy (SEM)

Scanning electron microscopy (SEM) analysis were performed using two instruments: (A) Environmental scanning electron microscopy (ESEM, FEG, FEI Quanta 200) and (B) high-resolution scanning electron microscopy (HR-SEM, Ziess Ultra-Plus FEG HR-SEM). Both were equipped with EDX (energy-dispersive X-ray), SE (secondary electron) and BSE (back-scattered electron) detectors. The powdered sample was dispersed in ethanol and the suspension was treated in an ultrasonic bath for 3 min. The suspension was then applied as a droplet on an adhesive C slice without additional coating.

2.2.6 Transmission electron microscopy (TEM)

Transmission electron micrographs (TEM) were obtained using a JEOL JEM 2100 at 200kV, in TEM and STEM mode. The powdered sample was dispersed in ethanol and the suspension was treated in an ultrasonic bath for 3 min. The suspension was then applied as a droplet on a copper grid without additional coating.

2.7 Illumination

2.7.1 Near UV range

UVA exposures at 365nm (Philips F15T8/BL 15W lamp, Amsterdam, Netherland), were used for 0-150 min, at a distance of 35 cm from the samples, equivalent to 2.7 J/cm^2. Radiation flow was 1.5mW/cm^2 as determined by UVA light meter type YK-37UVSD, (Radiometer, Copenhagen, Denmark).

2.7.2 VIS range

A VIS light source (Philips 15WT8/Daylight lamp, Amsterdam, Netherland) was used for 0-150 min, in a distance of 35 cm from the samples. The samples were covered by UV filter (clean-room filter), which absorbs radiation under 550 nm.

2.8 Photodegradation

2.8.1 Cytochrome C reduction assay Cytochrome C (Cyt-C) reduction assay was carried out in 24 well plates, each containing 2 ml of oxidized Cyt C solution (0.1 mM of Cyt-C in PBS buffer, pH 7.4) and 0-0.8 mg of Anatase NPs (A-NPs), stirred with a micro magnetic bar. The wells were exposed to a light source for up to 30 min. Dark conditions in the control wells were obtained by covering the wells with aluminum foil. Samples (1 ml) were withdrawn and the A-NPs were sedimented by centrifugation (Heraeus, Thermo Fisher Scientific, Waltham, MA) at 17,800 g for 15 min. Optical densities of the supernatants (0.5 ml) were determined at 450 and 550 nm using a Genesys 10S UV-VIS spectrometer (Thermo Fisher, Waltham, MA, USA) to follow Fe^{3+}Cyt-C reduction to Fe^{2+}Cyt C, the reference value of 23.65 OD at 550 nm for 1 mM reduced Cyt C was used [18]. A 24 well plate was placed on a magnetic stirrer and under UV, filtered VIS light or dark condition. Since Cyt C absorbs radiation in the UV region the experiment setup included a UV filter which is usually used for covering the well plate (clean-room filter).

Constant agitation of the solution was insured by a magnetic stirrer placed in each well. The plate was irradiated for 30 minutes, every 5 min, 0.5 ml samples were transferred to Eppendorf vials, which were centrifuged at 15000 rpm for 15 min in order to separate the catalyst. The supernatants from each vial (0.5 ml) were diluted two-fold with PBS and examined by UV-VIS spectrometer (Thermo, Genesys 10S) in the wavelength 200-800 nm.

2.8.2 Profenofos degradation. Stock solutions of PF 12 ppm were prepared: 5 µl of PF analytical standard in 1.0 ml of acetonitrile (HPLC grade). 0.25 ml of this solution was dissolved in 500 ml of distilled water. 20 ml glass vial that was placed on a magnetic stirrer and under (35 cm below) UV\VIS light source or dark condition were used. Each vial contained 10 ml of PF stock solution (12 ppm of PF in distilled water) and 3.75 mg of the catalyst (TiO_2, TiO_2-Ag). Constant agitation of the solution was insured by an orbital stirrer at 300 rpm. The PF degradation was sampled for 0-250 min, withdrawing 1.0 ml aliquots every 30 min. The samples were centrifuged at 15000 rpm in order to separate the catalyst form the PF solution and were used for the GC-MS and HPLC analyses.

2.9 GC-MS Analysis

The samples from section 4.3.1 were extracted in hexane 1:1 and 50 µl of the hexane extract was injected to GC-MS (Perkin Elmer Clarus 680 GC coupled to an MS detector Clarus 600T in electron ionization (EI, 70 eV) mode). The GC-MS oven was fitted with a HP 5 Column (Agilent 30m x 0.25mm x 0.25 µm). The chromatographic conditions were: oven temperature 40°C (for 4.1 min), increased to 290°C at 15°C/min; run time was 20.77 min; injector temperature 70°C for 2.5 min increased to 300 at 99 deg/min; detector temperature 200°C; injector split ratio 1:250 until 2.5 min and after a split-less mode. The samples were first analyzed in SCAN mode in order to select

the retention time and the ion for PF and 4-bromo-2-chlorophenol (BCP). Single Ion Monitoring function (SIM) was used, **table S1** depicts the retention time and selected ion for each compound.

2.10 HPLC Analysis

The samples from section 4.3.1 were analyzed using an Alliance waters 2690 high-performance liquid chromatography (HPLC) equipped with a PDA detector (Waters 996). 100 µl samples were injected onto a C18 Zorbax ODS column (5 µ 25x0.46 cm) at a rate of 1 ml/min, the oven temperature was 30 °C, monitored at 220 nm. The mobile phase was an isocratic combination of acetonitrile (80%), water (19.9%) and 0.1%trifluoroacetic acid. Analytical curve: Stock solutions of 12 ppm of PF and BCP were prepared (**Figure S1**). These stock solutions working solutions were used to prepare working solutions at 2, 4, 6, 8, 10 and 12 ppm of each compound. Next, 100 µl samples were analyzed by HPLC as described above.

2.11 Statistical analysis

All data are expressed as means ± standard error of the mean. Significant differences were assessed by P-value.

3 Results

3.1 Anatase structure of TiO_2 NPs is the most photoreactive form

In this section, we aimed to study the physicochemical properties and photocatalytic activity of TiO_2 in order to define the optimal forms which possess the highest surface area and ROS activity of the TiO_2 matrices. For that, several types of TiO_2 (anatase, rutile, amorphous) at the nano-size scale were examined by the Cyt C reduction assay (described in the Experimental Section) were used to assess the ROS production of the different TiO_2 preparations (A-NP, R-NP P-25) upon UVA illumination. As shown in **Figure 1A,** the most active form of TiO_2 is the anatase nanoparticles (A-NPs) as expected from the high surface areas, small particle size, high permeability, high surface ratio and retention [19]. Illumination under UVA without Ti-NPs showed negligible photolysis.

Next, we set to measure the ROS generation by A-NPs using the Cyt C reduction assay under the same illumination conditions. Optimization of A-NPs concentration in the ROS generation assay for 30 min is shown in **Figure 1B**. Based on these experiments, 0.4 mg/ml of A-NPs was chosen to study the rate of ROS production over time **(Figure 1C**).

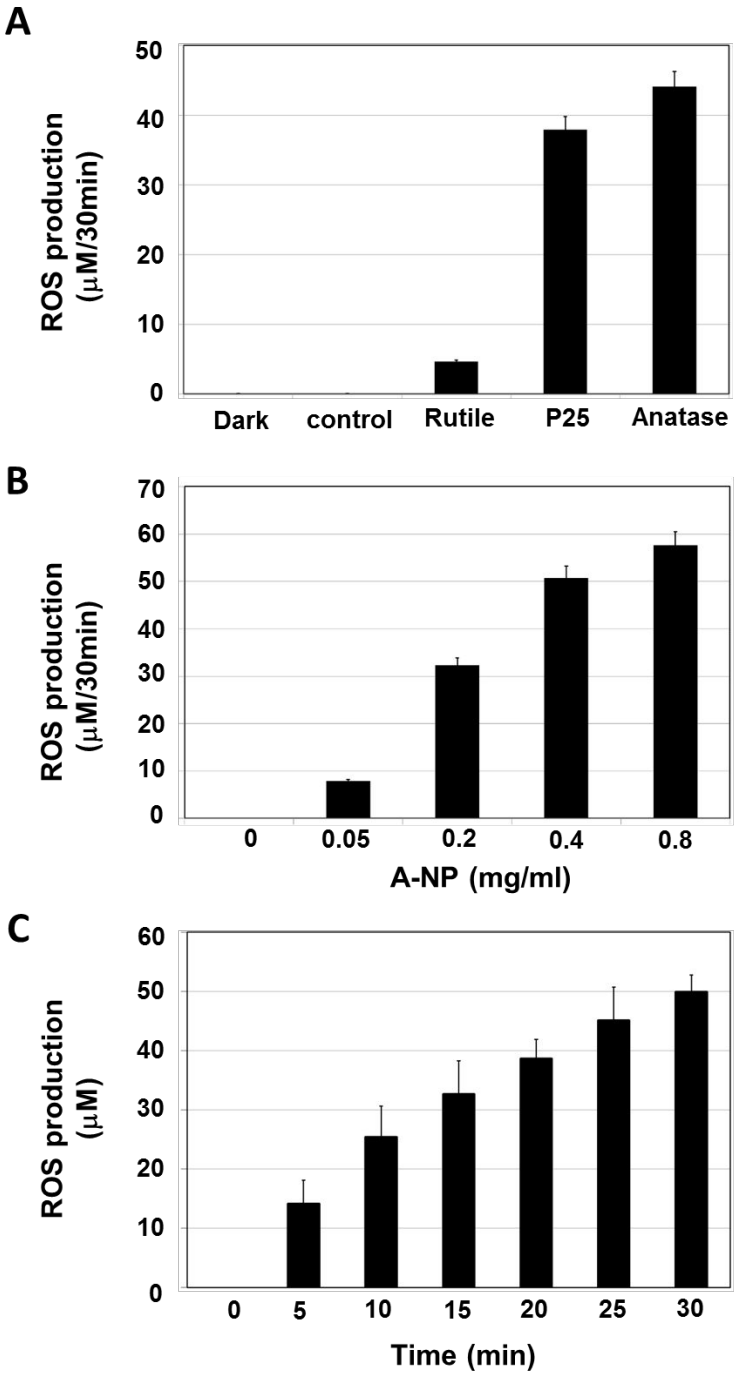

Figure 1 - The photocatalytic activity of TiO_2 forms and platforms upon UVA illumination as determined by the Cyt C assay. (A) ROS production by different TiO_2 structure after 30 min. **(B)** ROS production by amounts of A-NPs after 30 min measure. **(C)** Time dependence of ROS production by a constant amount of A-NPs (0.4 mg/ml). Experiments were repeated three times in triplicates.

3.2 Detoxification of PF using A-NPs under UVA illumination

Next, we set to examine A-NPs application for detoxification of hazardous materials. As a model, we used PF, an organophosphorus pesticide that inhibits AChE activity and is extremely toxic to living animals [20]. A biosensor of AChE activity was used to determine the residual toxic effect following PF degradation. **As** demonstrated in **Figure 2A,** PF was rapidly degraded by A-NPs under UVA illumination, 45% within 90 min, as shown by both biosensor and GC-MS analysis of the degradation products. **Figure 2B** depicts the GC-MS analysis of PF degradation products, including the positions of degraded bonds. It can be seen that the main degradation products are: 4-BCP, produced by the cleavage of P-O bond, and dipropyl disulfide (DPDS), which is a dimerized product of propyl mercaptan formed by the cleavage of the P-S bond in PF.

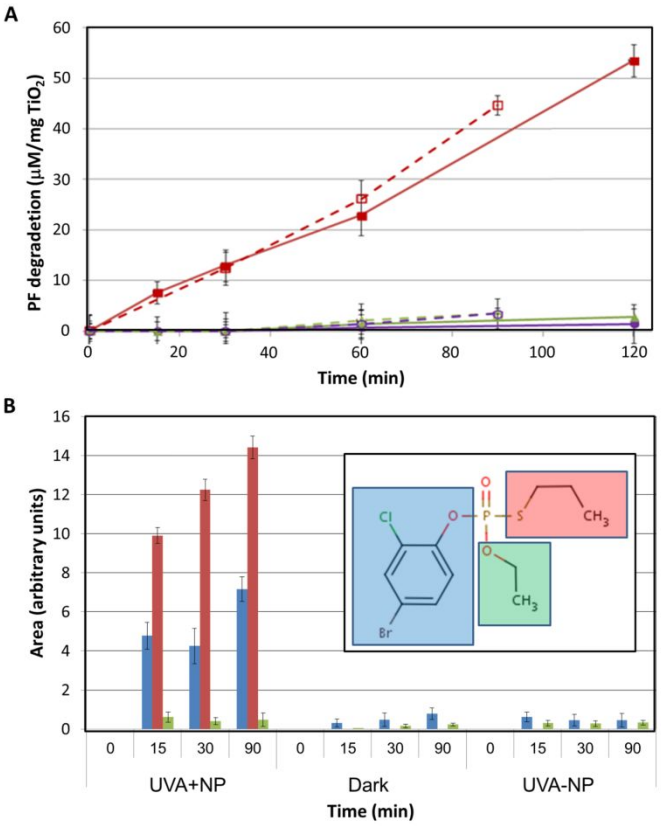

Figure 2 - PF degradation by A-NPs illumination. (A) Toxicity measured by inhibition of AChE activity (solid line) and degradation of PF measured by GC-MS (dashed line) under UV illumination (red lines) or in the absence of illumination (blue lines). The reaction with no TiO_2 particles is shown in green **(B)** GC-MS analysis of the reaction products of PF degradation – BCP – blue, DPDS – red and acetic acid - green.

3.3 TiO_2-modified by silver atoms for photocatalysis under VIS illumination

Attempts to increase TiO_2 photocatalytic activity by surface atomic metal dispersion is under extensive investigation. This approach is expected not only to increase photocatalysis under UV but also to allow activation at the VIS light range. Transition metal deposition on TiO_2 NPs, of silver atoms (Ag) in particular, has been reported

before in the literature [17]. We adopted this method to prepare a derivative of TiO_2-Ag by modifications of A-NPs with silver atoms (Ag).

Figure 3A shows different forms of TiO_2 surface (anatase, rutile and brookite) with atomic metal dispersion by Ag. The Ag clusters appear as white dots on the TiO_2 surface as shown on the right side panels of this figure, respectively. This preparation contains about 16-17% Ag on the surface of the A-NPs, as determined by XRD (**Figure 3B**). **Figure 3C** shows the %reflectence of TiO_2 different forms surface before (upper curves) and after modification by Ag (lower curves). As expected, the modifications of TiO_2 with Ag, led to the increase of absorbance (low reflectance) at the VIS range, followed by an increase in photoreactivity in this range (**Figure 3D**) at all TiO_2 modified forms, mostly with the anatase form.

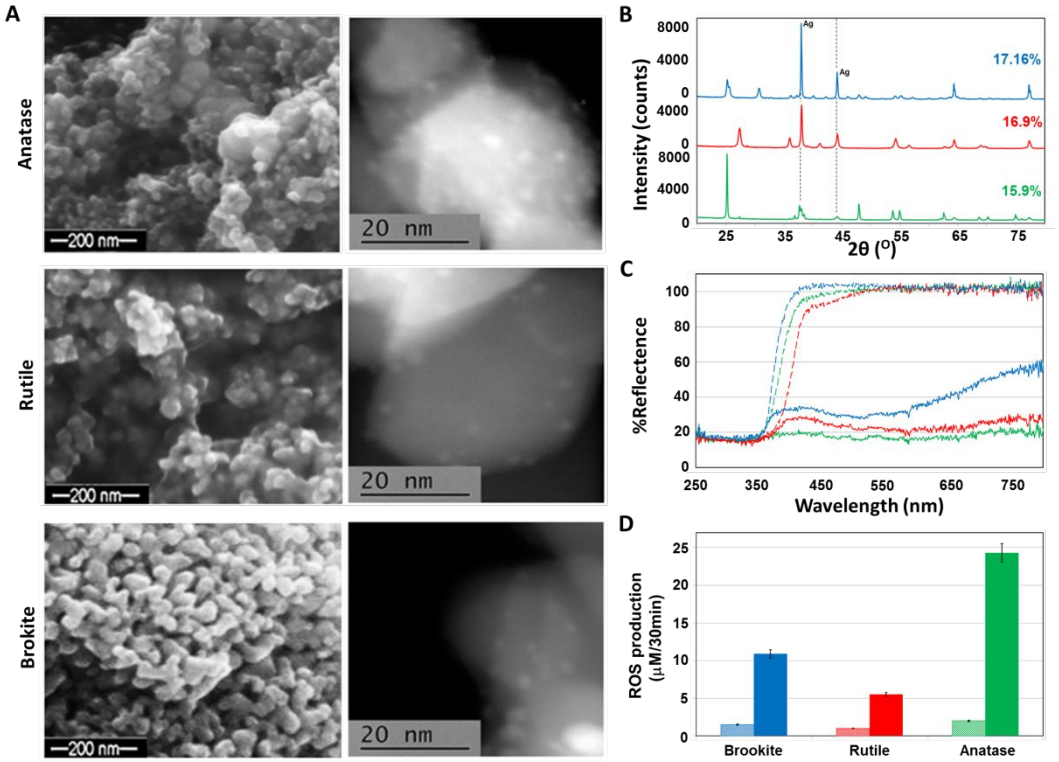

Figure 3 - TiO_2-Ag characterization. (A) ESEM micrograph of Ag-TiO_2, anatase (upper), rutile (middle) and brookite (lower). **(B)** XRD analysis of the TiO_2-NPs shown in figure 2A. **(C)** % Reflectance of TiO_2 forms; anatase (blue), rutile (red) and brookite (green) before (upper curve) and after (lower curve) modification with Ag. **(D)** Photoreactivity at the VIS range of TiO_2 forms before and after modification with Ag.

3.4 Detoxification of PF using A-NPs-Ag under VIS illumination

After it was established that the same results had been obtained with TiO_2-Ag under VIS light (data not shown), the samples were injected to HPLC and the concentration of BCP and PF were determined by comparing the peak area of the samples with the analytical curve. The kinetics of BCP accumulation was investigated under VIS illumination conditions. As shown in **Figure 4**, only TiO_2-Ag succeeds in generating ROS under VIS light while TiO_2 or Ag alone failed to do this. The kinetics profile is similar to that of the radicles generation indicating that the degradation may be attributed to the presence of radicals, including ROS. **Figure S2** depicts the photocatalytic activity of A-NPs-Ag under both illumination conditions, while the activity in the UV light region is much higher than VIS spectrum.

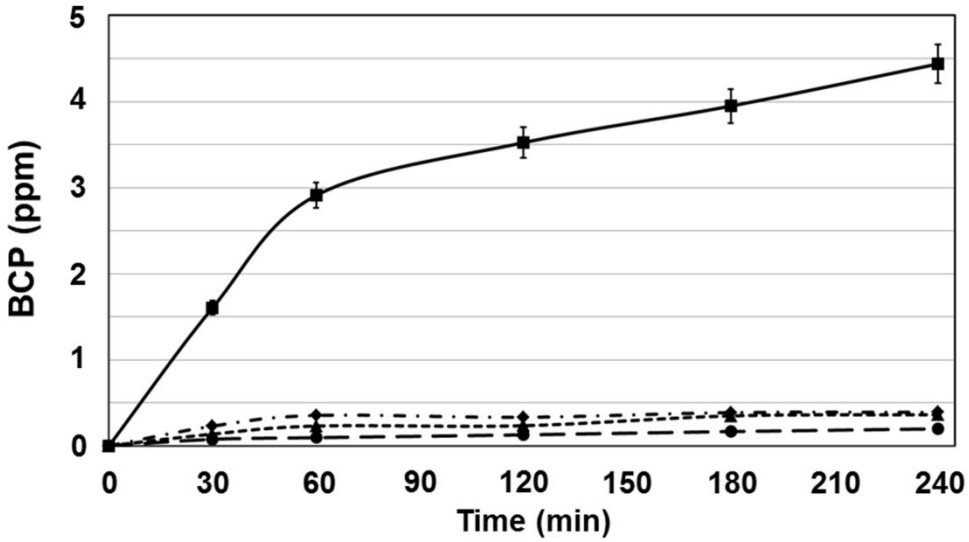

Figure 4 - Kinetics of BCP accumulation under VIS illumination using different catalysts. TiO_2-Ag (–■–),TiO_2 (–●), Ag (-▲-), non (–◆).

4 Discussion

The photocatalytic activity of TiO_2 under UV illumination is a well-studied process [9] and has been applied in many self-cleaning systems [6]. In this work, we identified that anatase nanoparticles (A-NPs) is the most photoreactive TiO_2 crystal structures form [10] with an optimized amount of 0.4 mg/ml that leading to increasing of ROS production with time upon UVA illumination, apparently resulted by the higher surface activity of anatase, compared to the rutile form [21]. Attempts to increase TiO_2 photocatalytic activity by metal doping, allowing activation at the VIS light range due to band-gap reduction [13] are currently under active research. Transitional metal deposition on TiO_2 NPs of silver atoms (Ag) in particular, has been reported earlier in the literature [17]. We adopted this method to prepare a derivative of Ag-TiO_2, by modifications of various TiO_2 forms with silver atoms and revealed that A-NPs is the most reactive form with optimization of 7.2% Ag concentration on the A-NPs surface. To note, neither TiO_2 alone nor Ag^+ alone, exhibit ROS production, which indicates that the enhancement of the photocatalytic activity is due to TiO_2-Ag and not to the silver itself.

PF was used as a surrogate for nerve gas, venomous agent X (VX), [2, 16] in order to demonstrate the ability of TiO_2 photodegradation of hazardous organic materials *in-situ* under UV or VIS illumination. Degradation processes by photocatalysis techniques were found efficient for many organics, including VX surrogates, in aqueous solutions [5, 22] and in films [23], but it requires direct contact with the agent. An alternative ROS generating technique is by vapor hydrogen peroxide or ozone which requires storage, transport, unique equipment, material disposable and may cause

damage for equipment. [24]. Therefore, the application of TiO_2-Ag at VIS range is more suitable for outdoor green decontamination.

TiO_2-Ag was found to degrade PF in aqueous solutions by cleavage of the P-S and the P-O bonds within few minutes under UV/VIS illumination as well as A-NPs at the UV spectrum. The degradation products firstly identified as BCP, formed by the cleavage of the P-O bond in PF, and DPDS, a dimerized form of propyl mercaptan formed by the P-S bond cleavage. As expected, the degradation of PF leads to its detoxification as shown electrochemically with an AChE activity sensor. In the presence of hydroxyl radicals, PF loss is expected to proceed mainly through hydrogen abstraction but the products identified here are different than those previously reported [2, 25], while biodegradation of PF using *Bacillus subtilis*, resulted similar degradation products [26].

5 Conclusions

The goal of this research was to develop and characterize a photodegradation system for toxic hazardous organic materials *in-situ* by TiO_2 and its derivatives. The decomposition of PF by several forms of TiO_2 via illumination at the UV range was studied. Reaction kinetics and products were identified as well as the detoxification effect. By modifying TiO_2 with Ag atoms, a doped complex of TiO_2-Ag was generated with the ability to produce ROS under VIS light illumination as well, which led to fast and high effective detoxification of PF.

Electronic Supplementary Material (ESM)

Supplementary material contains GC-MS data of the SIM-mode analyses (**Table S1**), BCP kinetics accumulation using A-NPs-Ag under VIS illumination conditions (**Figure S1**) and ROS production by A-NPs-Ag under different illumination conditions (**Figure S2**) are presented in the online version of this article at http: //dx.doi.org/10.1007/**********

Acknowledgements

The authors wish to express their gratitude to Professor Shachar Richter from the Faculty of Engineering at the Tel Aviv University) for his valuable advice and assistance in this project.

Notes and references

1. Mileson, B. E.; Chambers, J. E.; Chen, W.; Dettbarn, W.; Ehrich, M.; Eldefrawi, A.T.; Gaylor, D. W.; Hamernik, K.; Hodgson, E.; Karczmar, A. G. Common mechanism of toxicity: a case study of organophosphorus pesticides. *Toxicol. Sci.* **1998**, *41*, 8-20.
2. Petrick, L. M.; Sabach, S.; Dubowski, Y. Degradation of VX surrogate profenofos on surfaces via in situ photo-oxidation. *Environ. Sci. Technol.* **2013,** *47*, 8751-8758.
3. Štengl, V.; Houšková, V.; Bakardjieva, S.; Murafa, N.; Maříková, M.; Opluštil, F.; Němec, T. Zirconium doped nano-dispersed oxides of Fe, Al and Zn for destruction of warfare agents. *Mater. Charact.* **2010,** *61*, 1080-1088.
4. Wagner, G. W.; Koper, O. B.; Lucas, E.; Decker, S.; Klabunde, K. J. Reactions of VX, GD, and HD with nanosize CaO: autocatalytic dehydrohalogenation of HD. *J. Phys. Chem. B* **2000,** *104*, 5118-5123.
5. Vega, A. A.; Imoberdorf, G. E.; Mohseni, M. Photocatalytic degradation of 2, 4-dichlorophenoxyacetic acid in a fluidized bed photoreactor with composite template-free TiO2 photocatalyst. *Appl. Catal. A.* **2011,** *405*, 120-128.
6. Pelaez, M.; Falaras, P.; Likodimos, V.; Kontos, A. G.; Armah, A.; O'shea, K.; Dionysiou, D. D. Synthesis, structural characterization and evaluation of sol–gel-based NF-TiO2 films with visible light-photoactivation for the removal of microcystin-LR. *Appl. Catal. B.* **2010**, *99*, 378-387.
7. Elias, C. N.; Lima, J. H. C.; Valiev, R.; Meyers, M. A. Biomedical applications of titanium and its alloys. *J. Minerals, Metals, Mater. Soc.* **2008,** *60*, 46-49.
8. Felsovalyi, F.; Mangiagalli, P.; Bureau, C.; Kumar, S. K.; Banta, S. Reversibility of the adsorption of lysozyme on silica. *Langmuir.* **2011,** *27*, 11873-11882.
9. Fujishima, A.; Honda, K. Electrochemical photolysis of water at a semiconductor electrode. *Nature* **1972,** *238*, 37-38.
10. Zaleska, A. Doped-TiO2: a review. *Recent Pat. Eng.* **2008**, *2*, 157-164.
11. Zhu, W.; Qiu, X.; Iancu, V.; Chen, X.-Q.; Pan, H.; Wang, W.; Dimitrijevic, N. M.; Rajh, T.; Meyer III, H. M.; Paranthaman, M. P. Band gap narrowing of titanium oxide semiconductors by noncompensated anion-cation codoping for enhanced visible-light photoactivity. *Phys. Rev Lett.* **2009**, *103*, 226401-226404.
12. Liu, B.; Wen, L.; Zhao, X. The study of photocatalysis under ultraviolet+ visible two-beam light irradiation using undoped nano-titanium dioxide. *Mater. Chem. Phys.* **2008,** *112*, 35-40.
13. Park, H.; Park, Y.; Kim, W.; Choi, W. Surface modification of TiO2 photocatalyst for environmental applications. *J. Photochem. Photobiol. C: Photochem. Rev.* **2013,** *15*, 1-20.
14. Štengl, V.; Bakardjieva, S.; Murafa, N., Preparation and photocatalytic activity of rare earth doped TiO_2 nanoparticles. *Mater. Chem. Phys.* **2009**, *114*, 217-226.
15. Shah, P.; Ray, D. Profenofos. *Pestic. Residues Food—**2007,*** 403-443.
16. Malghani, S.; Chatterjee, N.; Hu, X.; Zejiao, L. Isolation and characterization of a profenofos degrading bacterium. *J. Environ. Sci.* **2009**, *21*, 1591-1597.
17. Li, M.; Noriega-Trevino, M. E.; Nino-Martinez, N.; Marambio-Jones, C.; Wang, J.; Damoiseaux, R.; Ruiz, F.; Hoek, E. M. Synergistic bactericidal activity of

Ag-TiO2 nanoparticles in both light and dark conditions. *Environ. Sci. Technol.* **2011**, *45*, 8989-8995.

18. Cunningham, M. L.; Johnson, J. S.; Giovanazzi, S. M.; Peak, M. J. Photosensitized production of superoxide anion by monochromatic (290–405 nm) ultraviolet irradiation of NADH and NADPH coenzymes. *Photochem. Photobiol.* **1985**, *42*, 125-128.

19. Bertrand, N.; Wu, J.; Xu, X.; Kamaly, N.; Farokhzad, O. C. Cancer nanotechnology: the impact of passive and active targeting in the era of modern cancer biology. *Adv. Drug Delivery Rev.* **2014**, *66*, 2-25.

20. Malghani, S.; Chatterjee, N.; Yu, X,; Zejiao, L. Isolation and characterization of a profenofos degrading bacterium. *J. Environ. Sci.* **2009**, *21,*1591–1597.

21. Van der Meulen, T.; Mattson, A.; Österlund, L. A comparative study of the photocatalytic oxidation of propane on anatase, rutile, and mixed-phase anatase–rutile TiO 2 nanoparticles: role of surface intermediates. *J. Catal.* **2007**, *251*, 131-144.

22. Vorontsov, A. V.; Chen, Y.-C.; Smirniotis, P. G. Photocatalytic oxidation of VX simulant 2-(butylamino) ethanethiol. *J. Hazard. Mater.* **2004**, *113*, 89-95.

23. Beduk, F.; Aydin, M. E.; Ozcan, S., Degradation of malathion and parathion by ozonation, photolytic ozonation, and heterogeneous catalytic ozonation processes. *CLEAN–Soil, Air, Water* **2012**, *40*, 179-187.

24. Nizkorodov, S. A.; Harper, W. W.; Blackmon, B. W.; Nesbitt, D. J., Temperature dependent kinetics of the OH/HO2/O3 chain reaction by time-resolved IR laser absorption spectroscopy. *J. Phys. Chem. A* **2000**, *104*, 3964-3973.

25. Foster, K. L.; Plastridge, R. A.; Bottenheim, J. W.; Shepson, P. B.; Finlayson-Pitts, B. J.; Spicer, C. W. The role of Br2 and BrCl in surface ozone destruction at polar sunrise. *Science* **2001**, *291*, 471-474.

26. Madhulika, K.; Verma, S.; Chatterjee, S. Profenofos, an acetylcholinesterase-inhibiting organophosphorus pesticide: a short review of its usage, toxicity, and biodegradation. J. Environ. Qual. **2016**, *45,* 1478-1489.

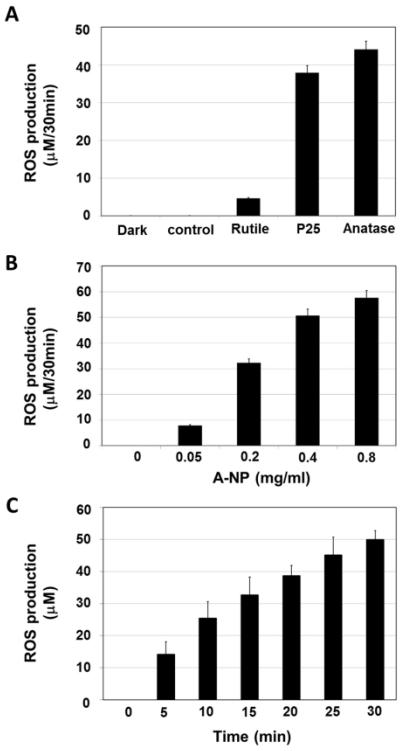

Figure 1 - The photocatalytic activity of TiO2 forms and platforms upon UVA illumination as determined by the Cyt C assay. (A) ROS production by different TiO2 structure after 30 min. (B) ROS production by amounts of A-NPs after 30 min measure. (C) Time dependence of ROS production by a constant amount of A-NPs (0.4 mg/ml). Experiments were repeated three times in triplicates.

254x190mm (300 x 300 DPI)

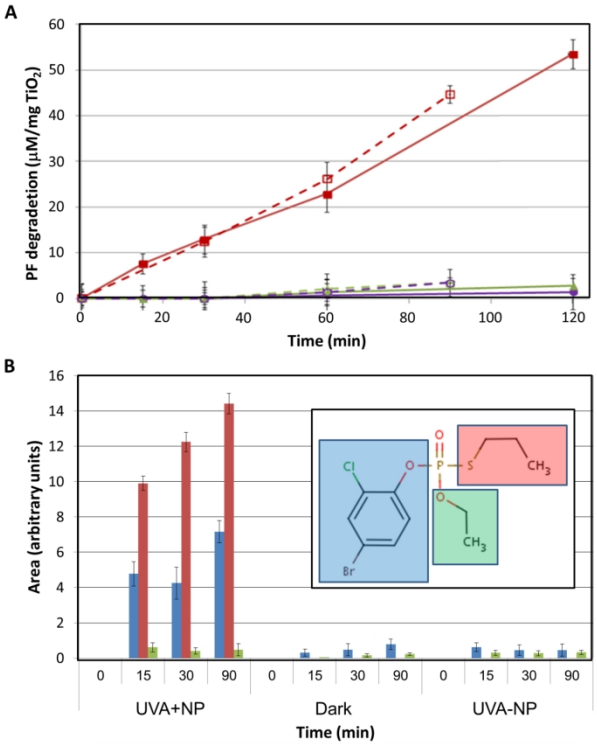

Figure 2 - PF degradation by A-NPs illumination. (A) Toxicity measured by inhibition of AChE activity (solid line) and degradation of PF measured by GC-MS (dashed line) under UV illumination (red lines) or in the absence of illumination (blue lines). The reaction with no TiO2 particles is shown in green (B) GC-MS analysis of the reaction products of PF degradation – BCP – blue, DPDS – red and acetic acid - green.

254x190mm (300 x 300 DPI)

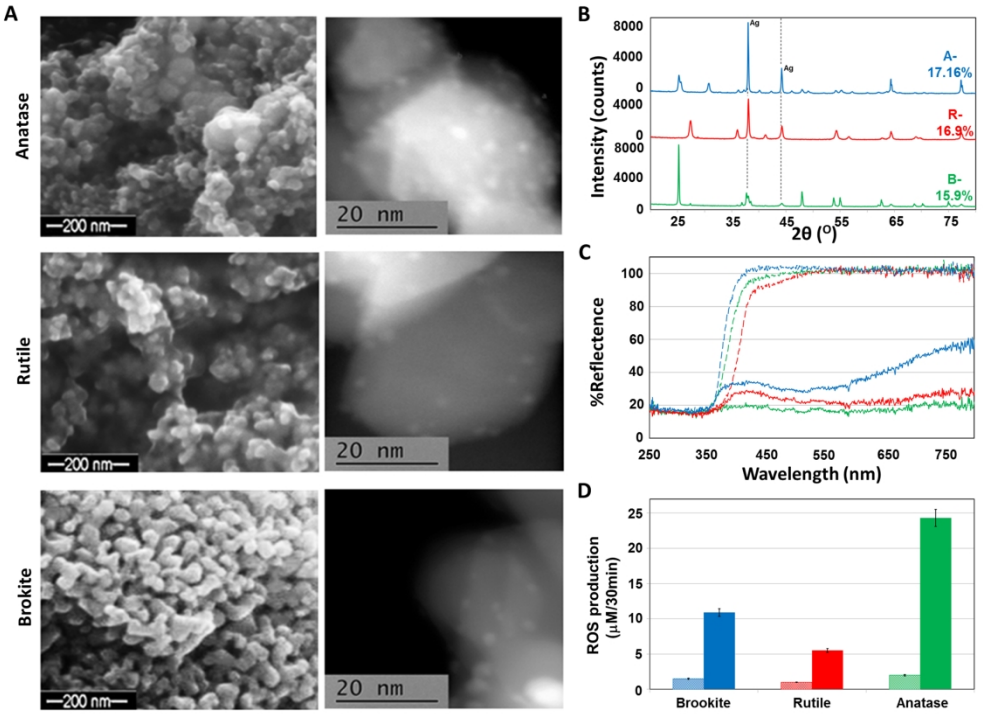

Figure 3 - TiO2-Ag characterization. (A) ESEM micrograph of Ag-TiO2, anatase (upper), rutile (middle) and brookite (lower). (B) XRD analysis of the TiO2-NPs shown in figure 2A. (C) % Reflectance of TiO2 forms; anatase (blue), rutile (red) and brookite (green) before (upper curve) and after (lower curve) modification with Ag. (D) Photoreactivity at the VIS range of TiO2 forms before and after modification with Ag.

254x190mm (300 x 300 DPI)

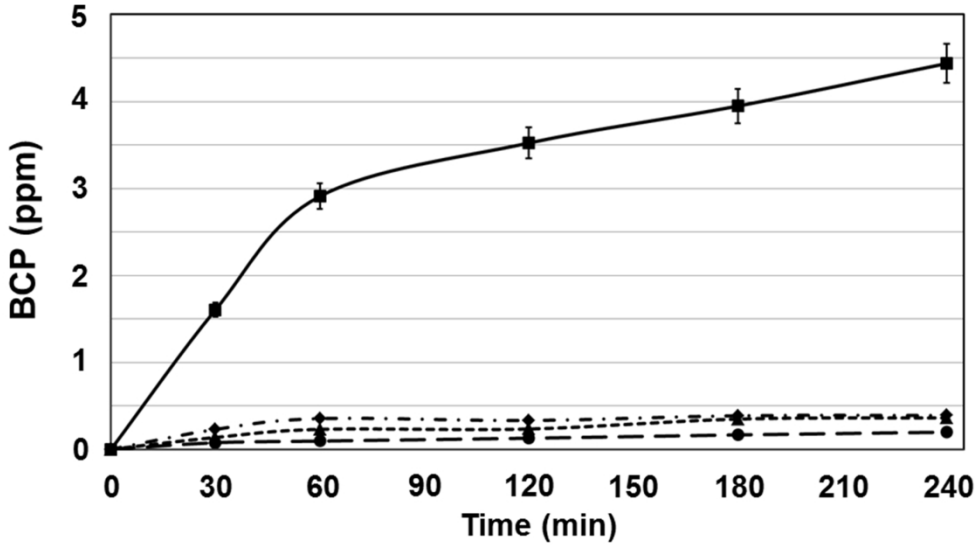

Figure 4 - Kinetics of BCP accumulation under VIS illumination using different catalysts. TiO2-Ag ( ),TiO2 ( ), Ag ( ), non ( ).

254x190mm (300 x 300 DPI)

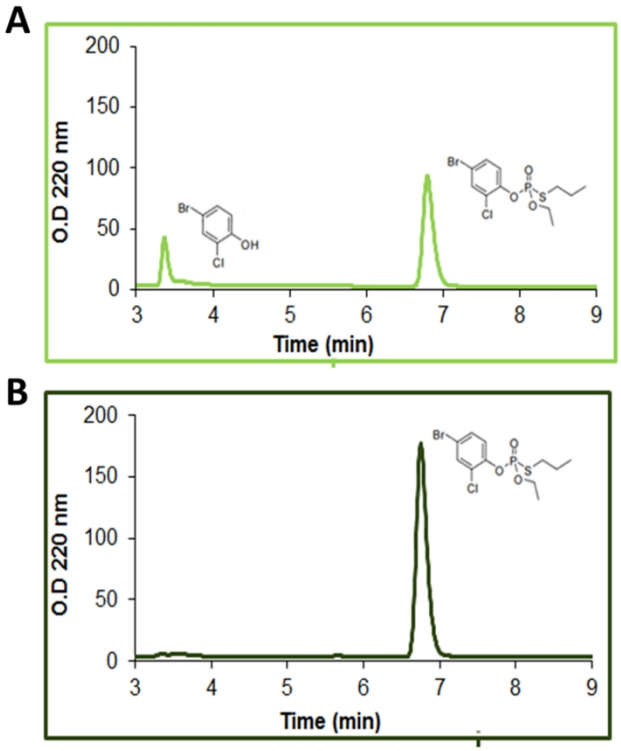

Figure S1 – BCP kinetics accumulation using A-NPs-Ag under VIS illumination conditions (A) or without (B).

254x190mm (300 x 300 DPI)

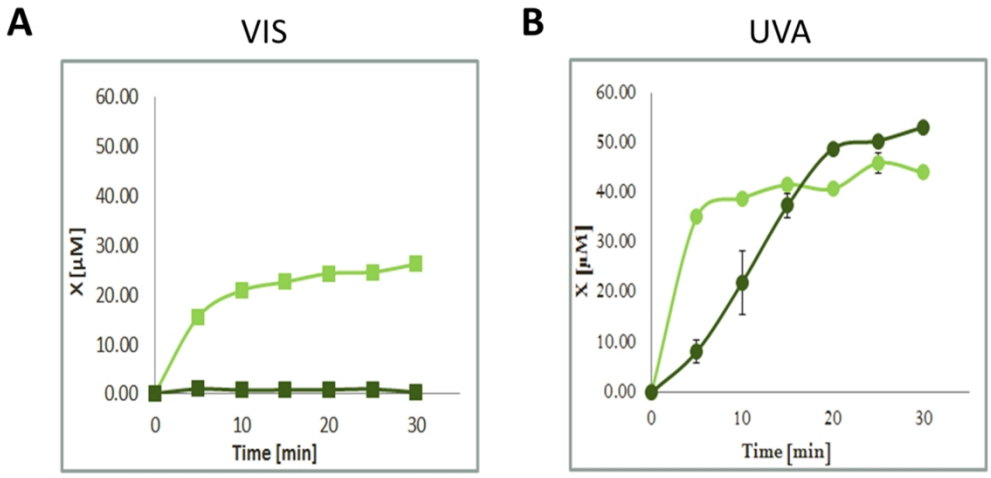

Figure S2 – ROS production by A-NPs-Ag under different illumination conditions. (A) VIS (B) UV.

254x190mm (300 x 300 DPI)